AIAA JOURNAL
Vol. 40, No. 10, October 2002

Fast Convergence of Viscous Airfoil Design Problems

Andrea Dadone*
Politecnico di Bari, 70125 Bari, Italy
and
Bernard Grossman†
Virginia Polytechnic Institute and State University, Blacksburg, Virginia 24061

An efficient formulation for the inverse and direct design optimization of airfoils in laminar and turbulent flow is presented. Our procedure simultaneously relies on converging the design process and the analysis, while sequentially using progressively finer grids. All flow analyses and the objective function are computed with standard accurate viscous flow solvers. Approximate design sensitivities are computed using a highly efficient adjoint solution procedure based on an artificially dissipative, inviscid auxiliary flow solver on a coarse grid. Our procedure involves what we term progressive optimization, whereby a sequence of operations, containing a partially converged flow solution, followed by a partially converged adjoint solution followed by an optimization step, is performed. This approach has been tested on several sample inverse and direct (constrained) design problems involving two-dimensional airfoils in laminar and turbulent flow conditions. The methodology has exhibited robustness and was shown to be highly efficient, with converged design optimizations produced in no more than the computational work to perform two flow analyses on the finest mesh, independent of the number of design variables.

Introduction

As discussed in Ref. 1, fluid dynamic design procedures generally require the calculation of many computationally expensive flow analyses. A series of papers have been written[1–5] on ways of reducing this computational burden. Most approaches to fluid dynamic design problems, as discussed in Ref. 1, are based on a sequence of global iterations, each one of them requiring a computation of the converged flowfield, a solution for the sensitivity derivatives, and an appropriate update of the design variables. The high computational cost of this serial approach comes principally from the repeated solution of flow equations. Reference 2 examines issues related to developing robust sensitivities using an adjoint formulation based on an approximate flow solver. The efficiency of the smoothing procedure suggested in Ref. 2 has recently been improved by introducing a progressive optimization strategy,[1,3,4] whereby the optimization process is based on partially converged flow solutions with the aim of converging the flow solution while converging the design problems. In addition, we also implement what we term mesh progressivity, whereby the aforementioned process is initiated on coarse grids and the grids are refined as the design solution converges.

In Ref. 1, several inverse design problems for two-dimensional inviscid flows have been efficiently solved, and both direct and inverse design problems for airfoils in inviscid flow conditions have been solved in Ref. 3. The progressive convergence strategy has been compared to serial convergence strategy in Ref. 1, where a two-dimensional transonic diffuser optimized by using seven design variables has been considered. It has been shown that the progressivity of the flow solution and the mesh progressivity resulted in a reduction of the computational effort by a factor of 50. A rough evaluation of the two contributions indicated that a factor varying from 2 to 4 results from the mesh progressivity and a factor ranging from 10 to 25 results from the flow solution progressivity.

Received 16 February 2001; revision received 12 March 2002; accepted for publication 14 March 2002.

*Professor, Dipartimento di Ingegneria Meccanica e Gestionale, Sezione Macchine ed Energetica. Senior Member AIAA.

†Professor and Department Head, Department of Aerospace and Ocean Engineering. Fellow AIAA.

For the two-dimensional design problems in Refs. 1 and 3, the adjoint equations were solved using a direct solver. The extension to three-dimensional inviscid flow problems has been considered in Ref. 4, where the progressive procedure suggested in Ref. 1 was modified by introducing an iterative solver of the adjoint equations, appropriate for three-dimensional flow problems. Specifically, the steady-state adjoint equations were transformed to pseudotime-dependent adjoint equations by introducing appropriate time derivative terms. These equations were solved in a progressive manner quite similar to the one employed for the flow equations. Direct and inverse transonic airfoil design problems, as well as inverse design problems of two- and three-dimensional transonic nozzles and three-dimensional supersonic blunt bodies, have been efficiently solved in Ref. 4. The introduction of the time-dependent adjoint equations, together with their progressive solution, enabled us to extend the efficiency of the methodology to three-dimensional problems.

The computation of the adjoint solutions only on coarse grids for inviscid flow problems in two and three dimensions has been introduced in Ref. 5, where many inverse design tests have been computed. These included numerous test cases on a transonic channels, transonic airfoils, transonic nozzles, and supersonic blunt bodies. The average saving in computational effort due to the computation of the adjoint variables on coarse grids ranged from 20 to 50%. Overall, the key elements of our procedure to date include the use of the auxiliary flow solver for the adjoint problem formulation, which contributes to robustness and the progressive convergence of the flow and adjoint solutions, together with the mesh progressivity, which contributes to efficiency.

The smoothing procedure,[2] the use of partially converged flow and adjoint equation solutions in the progressive optimization,[4] as well as the computation of the adjoint solutions on coarse grids,[5] imply that the optimization process is based on approximate values of the gradient of the objective function. Another example of approximate design sensitivity has been discussed by Matsuzawa and Hafez,[6] where adjoint equations based on an inviscid flow formulation have been used to determine approximate gradients of the objective function for airfoil inverse design in laminar flow conditions. Particularly, subsonic and transonic flow about a NACA 0012 airfoil at zero incidence have been considered, and the corresponding inverse design problems were successfully solved. A drawback of the methodology in Ref. 6, consistent with its serial approach, is the relatively large number of design cycles required to converge the optimization problem.

The recent work of Alexandrov et al.[7] examined procedures that utilized design information from coarse grid designs to efficiently

calculate designs on finer grids within a variable-complexity procedure that they call an approximation and model management optimization (AMMO) framework. They report performance gains of a speed-up factor of 2–3. In addition, Alexandrov et al.[8] have examined utilizing inviscid Euler solutions in a viscous design problem and obtained a speedup factor of five. These works,[7,8] performed independently of the present paper and differing considerably in the methodology, do confirm some of the findings of the present paper.

The aim of the present paper is to extend the progressive optimization procedure of Ref. 5 to inverse and direct design problems of airfoils in laminar as well as in turbulent flow conditions. The adjoint equations will be derived using an inviscid solver involving a traditional centered scheme with added numerical viscosity. The inviscid formulation will be used to preserve the simplicity of the adjoint equations. Moreover, additional time derivative terms will be introduced to solve the time-dependent adjoint equations progressively in time. Finally, the flow equations will be solved on a progressively finer mesh, whereas the adjoint equations will always be solved on the coarsest mesh. This will reduce the cost of the computation of the gradient of the objective function to a few percent of the total cost of the optimization procedure.

We will present our inverse design optimization procedure first, and we will utilize a transonic nozzle design problem to quantify the approximations implied in calculating design sensitivities from the solution of the adjoint equations on coarse grids. Then inverse design problems of airfoils in both laminar and turbulent flow conditions will be presented. Finally, the constrained direct design formulation will be outlined, and the direct design of airfoils in laminar, as well as in turbulent, flow conditions will be described.

Inverse Design

The present optimization technique is based on the following steps: First an appropriate basic flow solver is used that accurately resolves all important features of the flowfield to evaluate the objective function. Then an artificial viscosity, auxiliary flow solver is utilized only to evaluate smooth sensitivity derivatives through appropriate adjoint equations. In the following, we will define the objective function, and we will present our accurate basic flow solver along with our auxiliary inviscid flow solver. Then we will present the corresponding pseudotime-dependent discrete adjoint formulation, and we will introduce our progressive optimization strategy. Before we get to the major results of the paper, our optimization technique will be applied to the inverse design of a transonic inviscid two-dimensional nozzle, to outline the approximations implied in the solution of the inviscid adjoint equations on coarse grids. We will then describe the solution of several inverse design problems involving airfoils in laminar and turbulent flow conditions.

Objective Function

The inverse design of airfoils consists of finding the geometric shape whose pressure distribution along the wall $p(s, \boldsymbol{\xi})$ matches a target pressure distribution $\hat{p}(s)$, where s is the curvilinear coordinate measured along the surface and $\boldsymbol{\xi}$ corresponds to a set of design parameters. A discrete objective function I may be defined as

$$I(\xi_1, \xi_2, \ldots, \xi_n) = \frac{1}{2N_c}\sum_{i=1}^{N_c}[p_i - \hat{p}_i]^2 \tag{1}$$

where N_c is the number of intervals used to discretize the airfoil surface. The center locations of such intervals are indicated by s_i, $i = 1, \ldots, N_c$. The discrete computed pressures are $p_i = p(s_i, \xi_1, \xi_2, \ldots, \xi_n)$, and the discrete target pressures are $\hat{p}_i = \hat{p}(s_i)$, where ξ_j, $j = 1, \ldots, n$, represents the design parameters.

Navier–Stokes Solver

The two-dimensional Navier–Stokes equations in a Cartesian coordinate system can be written as

$$\frac{\partial \boldsymbol{q}}{\partial t} + \frac{\partial}{\partial x}(\boldsymbol{f} - \boldsymbol{f}_v) + \frac{\partial}{\partial y}(\boldsymbol{g} - \boldsymbol{g}_v) = 0 \tag{2}$$

The vector of the conserved variables is given by

$$\boldsymbol{q} = [\rho, \rho u, \rho v, \rho e_0]^T \tag{3}$$

and the convective terms of the flux vectors are

$$\boldsymbol{f} = \left[\rho u, p + \rho u^2, \rho uv, \rho u h_0\right]^T$$

$$\boldsymbol{g} = \left[\rho v, \rho uv, p + \rho v^2, \rho v h_0\right]^T \tag{4}$$

where u and v are the components of the velocity vector in the Cartesian coordinate system, and p, ρ, e_0, and h_0 represent the pressure, the density, the total energy, and the total enthalpy per unit mass. The shear stress and heat transfer terms of the flux vectors are given by

$$\boldsymbol{f}_v = [0, \tau_{xx}, \tau_{xy}, b_x]^T, \qquad \boldsymbol{g}_v = [0, \tau_{yx}, \tau_{yy}, b_y]^T \tag{5}$$

where, in Cartesian tensor notation,

$$\tau_{x_i x_j} = \left(\frac{\mu}{Re_L}\right)\left[\frac{\partial u_i}{\partial x_j} + \frac{\partial u_j}{\partial x_i} - \left(\frac{2}{3}\right)\left(\frac{\partial u_k}{\partial x_k}\right)\delta_{ij}\right]$$

$$b_{x_i} = u_j \tau_{x_i x_j} - \dot{q}_{x_i} \tag{6}$$

Moreover,

$$\dot{q}_{x_i} = -\frac{[\mu(\partial T/\partial x_i)]}{\left[(\gamma - 1)Re_L Pr M_r^2\right]}, \qquad Re_L = \frac{\bar{\rho}_r \bar{q}_r \bar{L}}{\bar{\mu}_r}$$

$$M_\infty = \frac{\bar{q}_r}{\bar{a}_r}, \qquad q = \sqrt{u^2 + v^2} \tag{7}$$

where T, Pr, μ, and γ are the temperature, the Prandtl number, the viscosity, and the specific heat ratio, respectively. The preceding equations have been nondimensionalized with respect to reference values of length $\bar{L}$, density $\bar{\rho}_r$, temperature $\bar{T}_r$, velocity $\bar{q}_r$, and viscosity $\bar{\mu}_r$.

A semidiscrete finite volume representation of Eq. (2) leads to

$$\Delta V \frac{\partial \hat{\boldsymbol{q}}}{\partial t} + \sum[(\boldsymbol{F} - \boldsymbol{F}_v)\Delta S] = 0 \tag{8}$$

where the vector $\hat{\boldsymbol{q}}$ indicates the average value of the vector $\boldsymbol{q}$ in the cell volume ΔV and ΔS indicates the cell face area, with the summation over all cell faces. Finally,

$$\boldsymbol{F} = (\boldsymbol{f}\hat{i}_x + \boldsymbol{g}\hat{i}_y)\cdot \hat{n}, \qquad \boldsymbol{F}_v = (\boldsymbol{f}_v\hat{i}_x + \boldsymbol{g}_v\hat{i}_y)\cdot \hat{n} \tag{9}$$

where $\hat{n}$ is the unit vector normal to the considered cell face, whereas $\hat{i}_x$ and $\hat{i}_y$ represent the unit vectors associated with the Cartesian coordinate system.

The convective terms have been discretized with the flux-difference-splitting method of Roe.[9] A MUSCL-type extrapolation[10] with a formal second-order accuracy in space has been applied to extrapolate the physical variables onto the left and right sides of each cell edge. The Van Albada et al. limiter[11] has been used to compute oscillation-free solutions. The heat flux and shear stress terms have been discretized through a central scheme employing Green's theorem. For turbulent flow computations, the eddy viscosity hypothesis has been assumed using the algebraic model of Baldwin and Lomax[12] with the Degani and Schiff[13] modification. The computational flowfield has been divided into an $N \times M$ finite volume mesh, where N indicates the intervals used in the body-wise direction and M the intervals in the direction normal to the body.

Auxiliary Flow Solver

The auxiliary inviscid flow solver is used only for the approximate computation of smooth sensitivity derivatives, that is, as in Ref. 2, via a discrete adjoint formulation. It must be characterized by added artificial viscosity to smooth the shock. Furthermore, we wish to utilize an inviscid flow solver to preserve the simplicity of the adjoint equations (although an additional level of approximation

is introduced in the computation of the adjoint variables). The simplest approach that will meet our goals is to use a central scheme with an adequate level of artificial viscosity. The requirements of the auxiliary solver allow the use of a simple, constant artificial viscosity μ. Numerical experiments have shown that a value of μ equal to 0.1 is appropriate in the coarsest grid computations that will be presented, whereas the value of μ has been proportionally increased in the finer grid calculations. The present auxiliary flow solver is used only in the discrete adjoint formulation, which is considered in the following.

Discrete Adjoint Formulation

The technique presented in Ref. 1 gives the following equation for the computation of the derivatives of the objective function:

$$\frac{\partial I}{\partial \xi_j} = \left(\frac{\partial I}{\partial \xi_j}\right)_u - \Lambda_k^T \left(\frac{\partial \boldsymbol{w}_k}{\partial \xi_j}\right)_u \tag{10}$$

where the adjoint variables Λ_k are evaluated according to the following conditions:

$$\left(\frac{\partial \boldsymbol{w}_k}{\partial \boldsymbol{u}_i}\right)_\xi^T \Lambda_k = \left(\frac{\partial I}{\partial \boldsymbol{u}_i}\right)_\xi^T \tag{11}$$

for $i = 1, \ldots, N \times M$ and $j = 1, \ldots, n$, with n the number of design parameters, with repeated indices summed over their range. In the preceding equations, $\boldsymbol{u}_i$ corresponds to the vector of the physical variables at each cell center i:

$$\boldsymbol{u}_i = [p, \rho, u, v]_i^T \tag{12}$$

whereas $\boldsymbol{w}_k(\boldsymbol{u}, \boldsymbol{\xi}) = 0$ represents the discretized system of governing partial differential equations corresponding to the auxiliary inviscid flow solver.

In the present formulation, Eqs. (11) are modified by introducing additional terms representing the time derivative $\partial \Lambda_i / \partial t$ of the adjoint variables:

$$\frac{\partial \Lambda_i}{\partial t} + \left(\frac{\partial \boldsymbol{w}_k}{\partial \boldsymbol{u}_i}\right)_\xi^T \Lambda_k = \left(\frac{\partial I}{\partial \boldsymbol{u}_i}\right)_\xi^T \tag{13}$$

Equations (13) represent the adjoint equations, a set of $4 \times N \times M$ linear, algebraic time-dependent equations. In addition, the analytical expression of the terms $(\partial \boldsymbol{w}_k / \partial \boldsymbol{u}_i)_\xi$ and $(\partial \boldsymbol{w}_k / \partial \xi_j)_u$ can generally be determined directly from the definition of the system of algebraic equations, $\boldsymbol{w}_k = 0$.

The fluid dynamic variables computed with the accurate, basic Navier–Stokes flow solver are used to evaluate the terms $(\partial I / \partial \boldsymbol{u}_i)_\xi$ and $(\partial \boldsymbol{w}_k / \partial \boldsymbol{u}_i)_\xi$. Then, the adjoint equations are solved for the adjoint variables Λ_i, iterating in time. The computed fluid dynamic variables also allow the computation of the terms $(\partial I / \partial \xi_j)_u$ and $(\partial \boldsymbol{w}_k / \partial \xi_j)_u$. Finally, the sensitivity derivatives of the objective function, $\partial I / \partial \xi_j$, can be computed.

For the present two-dimensional application, Eq. (11) can be used to evaluate the adjoint variables with a direct flow solver, which has already proven to be efficient.[1] Generally, direct flow solvers cannot be used in three-dimensional applications because of excessive memory requirement. Thus, we have chosen the pseudotime-dependent iterative solver for the adjoint equations.

It is common practice to solve the adjoint equations on the same mesh employed for the solution of the flow equations, to obtain a mesh converged solution for the adjoint equations as well as for the flow equations. In this paper, we assess the impact of evaluating the solution of the adjoint equations with several approximations. One of these approximations involves solving the adjoint equations on a much coarser grid than the flow equations. We have found, based on numerical experiments, that sufficiently accurate adjoint solutions can be obtained on coarse grids provided that we evaluate the right-hand side of Eq. (13) and the coefficient term using accurate flow solution data. This coarse-grid evaluation of the adjoint variables has the impact of drastically reducing the computational time. In the following section, we will assess the impact of this approximation by case studies with an inviscid solution. Note that the inviscid test case is used to avoid the influence of the other adjoint approximation discussed in this paper involving the use of adjoint equations based on an inviscid flow solver for the optimization of viscous flow problems.

As far as the practical application of the procedure is concerned, the best approximation of the term $(\partial I / \partial \boldsymbol{u}_i)_\xi$ obviously gives the best approximated values of the adjoint variables. Therefore, this term is evaluated on the fine grid employed for the flow computation and then averaged and transferred to the coarse grid employed for the computation of the adjoint variables. Similarly, the conserved variables $\boldsymbol{q}$, corresponding to the flowfield computed on the finest mesh, will be appropriately averaged to determine the corresponding averaged flow solution on the coarse mesh employed for the computation of the adjoint variables. These averaged values will be used to evaluate the term $(\partial \boldsymbol{w}_k / \partial \boldsymbol{u}_i)_\xi$. The adjoint variables are then computed on the coarse grid. Finally, the sensitivity derivatives are computed by evaluating $(\partial I / \partial \xi_j)_u$ and $(\partial \boldsymbol{w}_k / \partial \xi_j)_u$ on the coarse grid.

Progressive Optimization Strategy

The goal of the present convergence technique is to determine simultaneously the minimum of the objective function, while progressively reaching a converged solution for the flowfield.

The progressive algorithm consists of the following steps:

1) Start with an initial set of design variables.

2) Start the flow computations on a coarse grid.

3) Advance the flow solver for several iterations.

4) Evaluate the adjoint equations on the coarse grid by advancing the adjoint solver for several iterations, with the condition that the residuals drop at least one order of magnitude with respect to its value at the beginning of the procedure.

5) Compute the objective function gradient ∇I.

6) Update the design variables according to the relation

$$\xi_j^{l+1} = \xi_j^l - a_j \frac{\partial I}{\partial \xi_j} \tag{14}$$

where a_j are positive parameters.

7) Repeat steps 3–6 until the gradient of the objective function is sufficiently decreased (from one to two orders of magnitude).

8) Refine the mesh by doubling the number of intervals in each direction and interpolate the computed flow solution to the finer grid.

9) Repeat steps 3–6 until the gradient of the objective function is decreased one-half to one order of magnitude more, the adjoint equations always being solved on the coarse grid.

10) Repeat steps 8 and 9 until the finest grid is reached.

11) Repeat steps 3–6 until the objective function has sufficiently decreased, the adjoint equations always being solved on the coarse grid.

The coefficient a_j in Eq. (14) is evaluated as $a_j = bc_j$. The coefficient b represents the minimum value of a_j and is given by

$$b = \frac{\Delta \xi_c}{k |\nabla_j I|^0_{\max}} \tag{15}$$

where $\Delta \xi_c$ is a typical (order of magnitude) change of the design parameters, k is a constant ranging from 40 to 100 depending on the test case, and $|\nabla_j I|^0_{\max}$ is the largest absolute value assumed by the sensitivity derivatives of the objective function after the first global step, steps 1–5. The term c_j is an amplification factor with a minimum value equal to 1 and a maximum value c_M that depends on the convergence of the normalized gradient of the objective function. Specifically, c_M is equal to 10 if the convergence is lower than one order of magnitude, is equal to 40 if it is higher than two orders, and it varies linearly between 10 and 40 for intermediate values of the convergence of the normalized gradient of the objective function. At the beginning of the computations, c_j is set to 1, and then it is increased by 50% if the corresponding sensitivity derivative of the objective function maintains its sign, whereas it is decreased by 50% if the sign changes. This approach allows large changes for the design variables whose sensitivity derivatives maintain the same sign, whereas it assigns small changes to design variables whose

sensitivity derivatives are changing their sign. We have devised this technique because of the very slow convergence of the method of steepest descent, corresponding to c_j equal to one. Our approach of using an inviscid smoothed adjoint solver for a viscous problem, together with the computation of the adjoint equations on a coarse grid and with our progressive optimization (where the flow and the adjoint solvers may be partially converged), leads to an approximate gradient evaluation, which caused convergence problems with classical optimizers. The use of the amplification factor c_j just described significantly improves convergence compared to the method of steepest descent.

In the computed results, we considered the objective function to have decreased sufficiently when the norm of its gradient has decreased 2.5 orders of magnitude with respect to its value after the first global step, steps 1–5.

The progressive optimization strategy has been extensively investigated for a variety of other problems that incorporated the same optimizer described earlier, Eq. (14), that utilized Eq. (15) to define the coefficient b with the terms k and c_j as defined earlier. Design problems using this optimization strategy included inviscid transonic flows in channels and about airfoils[5] as well as inviscid[14] and turbulent[15] transonic flows inside cascades. In addition, the progressive-mesh/progressive-convergence strategy has also been applied to the design of an industrial afterburner[16] using a commercial analysis code and computing the sensitivities by means of finite differences. The same optimizer was used without modifications and with all of the implied coefficients defined here.

Inviscid Two-Dimensional Nozzle Results

This test case is only presented to evaluate the approximation connected with using the coarse grid solution of the adjoint equations to evaluate sensitivities on fine grids in an inviscid design problem. Later in the paper we will be using inviscid, coarse grid sensitivities in viscous design problems. It is useful to evaluate these approximations separately.

The test case is the inviscid transonic flow in a symmetric nozzle. Calculations are performed on the lower half of the nozzle. The ordinates y_w of the lower wall corresponding to the nozzle profile are zero for $-0.5 \le x \le 0$ and $1 \le x \le 1.5$, whereas in the range $0 \le x \le 1$ they are defined as follows[17]:

$$y_w(x) = \sum_{i=1}^{N_a} \alpha_i x^{i+1}(x-1)^2 \tag{16}$$

The quantities α_i are the design parameters. The symmetry line is located at $y = 1$, and the outlet pressure is equal to 0.7.

We have considered $N_a = 20$ design variables. The target geometry corresponds to $\alpha_1 = 2.0$ and other α_i values equal to 0.5. The flowfield is evaluated by employing an H grid defined by $(x_l, y_n) = (x_o + l\Delta x, y_w + n\Delta y)$, where Δx is constant and Δy is a constant fraction of the local height of the channel. The computed pressure distribution on the lower wall of the target geometry is taken to be the target pressure.

The Mach number contour lines corresponding to the target bump geometry are shown in Fig. 1, where a small supersonic flow bubble located in the bump region and terminated by a recompression shock can be observed.

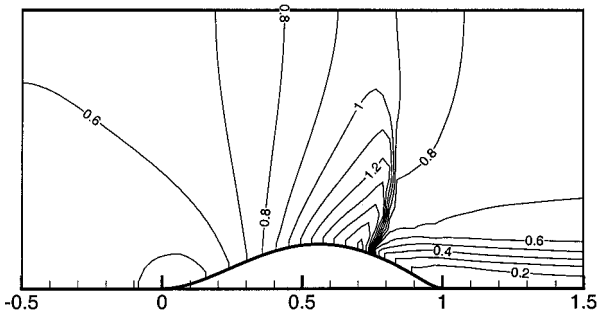

Fig. 1 Iso-Mach lines; inviscid two-dimensional nozzle.

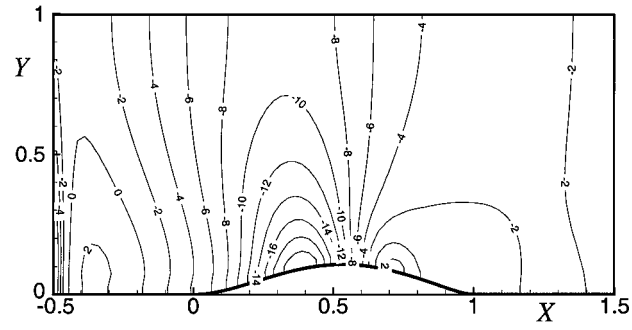

Fig. 2 Isolines of first adjoint variable Λ_1 (scaled by 1000); inviscid two-dimensional nozzle, mesh: 80 × 20 cells.

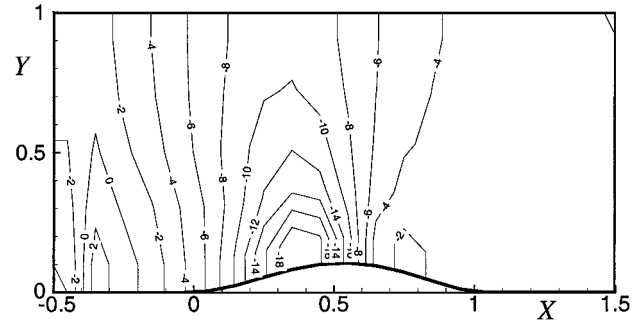

Fig. 3 Isolines of first adjoint variable Λ_1 (scaled by 1000); inviscid two-dimensional nozzle, mesh: 20 × 5 cells.

The initial values of the design parameters have been set such that $\alpha_1 = 1.5$, with the other α_i set to 0.2. The flow solver has then performed 1000 iterations on a mesh made by 80×20 cells. The incompletely converged flow solution has been used to compute the converged solution of the adjoint equations on the same mesh. The isolines corresponding to the first adjoint variable Λ_1, appropriately scaled by a factor of 1000, are plotted in Fig. 2. The same flow solution has then been used to compute the converged adjoint solution on a coarser mesh made by 20×5 cells. The isolines of the first adjoint variable Λ_1, computed on the coarser mesh, are plotted in Fig. 3. We note that the differences between the isolines are small. The adjoint variables computed with the coarse mesh give a reasonable representation of the adjoint field, although with some approximation. The gradient of the objective function has been also computed with the two different mesh distributions. In comparison with the value computed by employing the finer mesh, the modulus of the gradient of the objective function reduces by 4% if the coarser mesh is considered. Some other test cases have also been considered involving different initial values of the design parameters and different levels of convergence of the flow solution. All of the test cases have shown results very similar to those outlined here. Based on these results, we conjecture that computing the adjoint variables on coarser mesh distributions results in only a small error in the computation of the sensitivity derivatives. However, the computational time is reduced by more than two orders of magnitude, which means reducing the computational time to evaluate the sensitivity derivatives to less than 1% of the total computational time for the optimization process.

Laminar Flow Airfoil Results

The inverse design of airfoils in laminar flow conditions is considered here. Following the procedure used in Ref. 18, the airfoil surface shape is described as

$$Y\left(\frac{x}{c}\right) = \sum_{i=1}^{N_a} \alpha_i Y_i\left(\frac{x}{c}\right) \tag{17}$$

where $Y = y/c$, with y being the airfoil ordinate, and c the airfoil chord length. The shape functions $Y_i(x/c)$ are the ordinates of the N_a specified airfoils, which depend on the nondimensional

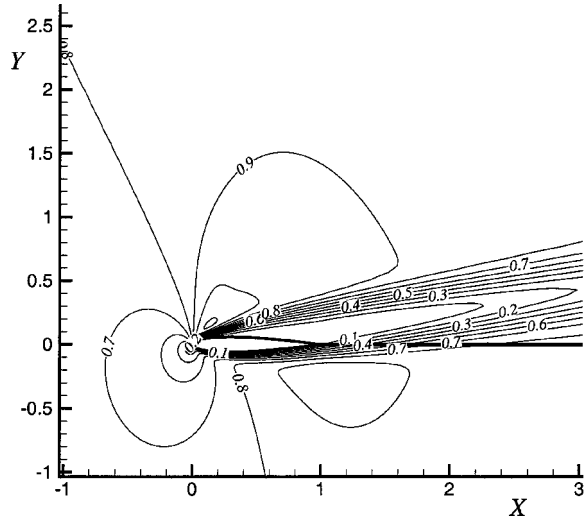

Fig. 4 Iso-Mach lines; laminar airfoil, finest mesh: 256 × 64 cells.

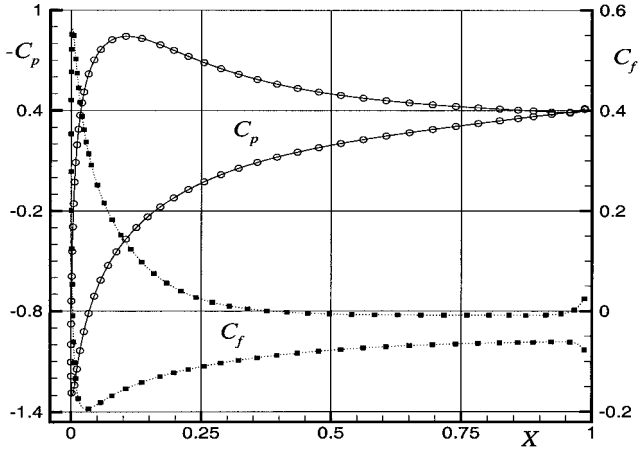

Fig. 5 Pressure and skin-friction coefficient distributions; laminar airfoil inverse design.

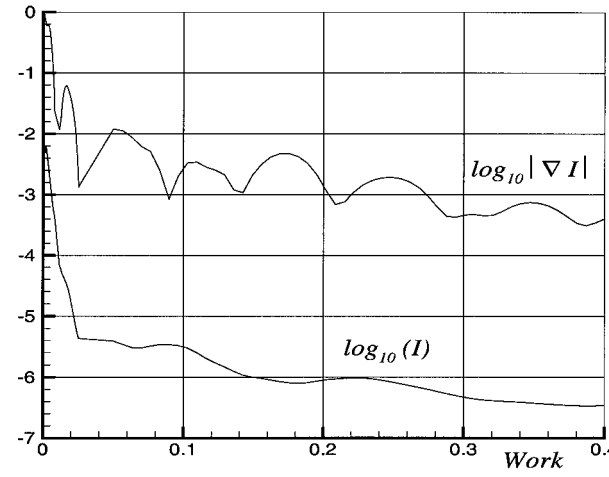

Fig. 6 Convergence history; laminar airfoil inverse design, finest mesh: 256 × 64 cells.

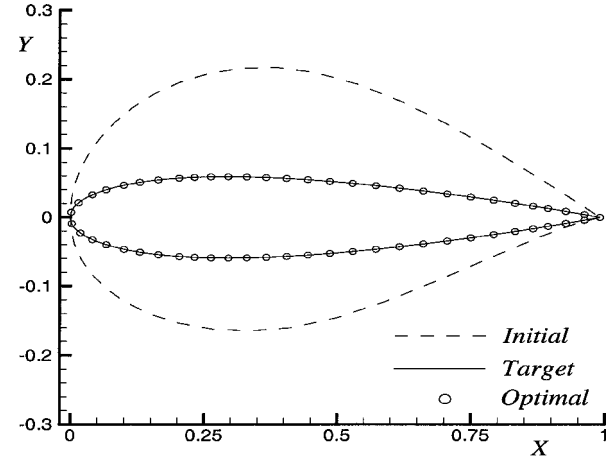

Fig. 7 Airfoil shapes; laminar airfoil inverse design.

abscissa x/c. The weighting terms α_i are the design parameters of the problem.

We considered the transonic laminar flow about a NACA0012 airfoil with an undisturbed Mach number $M_\infty = 0.80$, an angle of attack equal to 10 deg, and a Reynolds number equal to 5×10^2 (c.f., Ref. 19). Then the converged flowfield is evaluated by employing a C grid consisting of 256 × 64 cells. The computed Mach number contours are plotted in Fig. 4. In Fig. 5, we present the distribution of surface pressure coefficient (solid lines) and the distribution of skin-friction coefficient (dotted lines). The results in Figs. 4 and 5 are in good agreement with the well-assessed results reported in Ref. 19. The computed pressure distribution on the airfoil surface is taken to be the target pressure. Although this case does not have a shock, it may be considered a severe test case because the results of Figs. 4 and 5 indicate a large recirculation region on the upper surface of the airfoil.

We performed an optimization test with $N_a = 4$ and Y_1–Y_4 as the shape of four specified airfoils, NACA 0012, NACA 64_1-412, NACA 64_2A215, and NACA 65_2-415. The target set of coefficients is $\alpha = (1, 0, 0, 0)$, and we assumed an initial airfoil shape corresponding to the set of coefficients $\alpha = (1.5, 0.5, 0.5, 0.5)$. The optimization process has been performed by employing three mesh levels made by 64 × 16, 128 × 32, and 256 × 64 cells.

Figure 6 shows the convergence history of the logarithm (base 10) of the objective function, $\log_{10}(I)$, and of the logarithm (base 10) of the normalized gradient of the objective function, $\log_{10}|\nabla I|$. The abscissa in Fig. 6 is the required work, with a unit of work considered as the computational time required to run a single analysis on the finest mesh with a drop in the residuals equal to five orders of magnitude. The results indicate that the work required to converge the gradient of the objective function by 2.5 orders of magnitude is equal to 0.19 work units. This extremely efficient result is connected with the benefit of the mesh sequencing, which brings the optimization problem very close to convergence on the intermediate mesh. Therefore, very few expensive iterations are required on the finest mesh level. This is possible because of the absence of a shock in the flowfield. Another contributing factor is the use of the coarsest mesh to compute the adjoint variables. Indeed, the cost of the computation of the sensitivity derivatives is only 4% of the required computational work in the present test case.

The corresponding optimal distributions of the pressure coefficient and of the skin-friction coefficient are plotted in Fig. 5 as symbols. Figure 5 indicates the effective agreement between the target and the optimal distributions, including the skin-friction coefficient, indicating that the solution has converged sufficiently. Another indication of sufficient convergence can be observed in Fig. 7, where the target airfoil shape (continuous line) is plotted together with the initial airfoil shape (dashed line) and the optimized airfoil shape (symbols). Figure 7 shows that the optimized airfoil shape practically coincides with its target value. Figure 7 also illustrates that the optimization process starts from an airfoil shape that is very different from the optimized one. However, the optimization process reaches the target shape without being trapped at any other local minimum.

To analyze the influence of the mesh size, the preceding optimization process has been repeated by employing three coarser mesh levels made by 32 × 8, 64 × 16, and 128 × 32 cells. The initial and target α values were not changed. The corresponding convergence results indicate that the work required to converge the gradient of the objective function by 2.5 orders of magnitude, is equal to 0.37 work

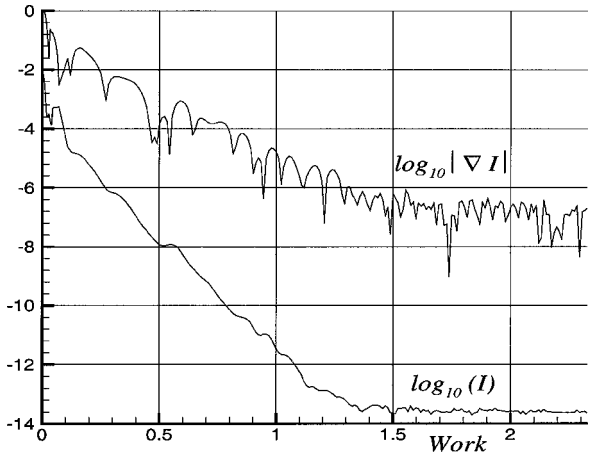

Fig. 8 Complete convergence history; one design variable laminar airfoil, finest mesh: 128 × 32 cells.

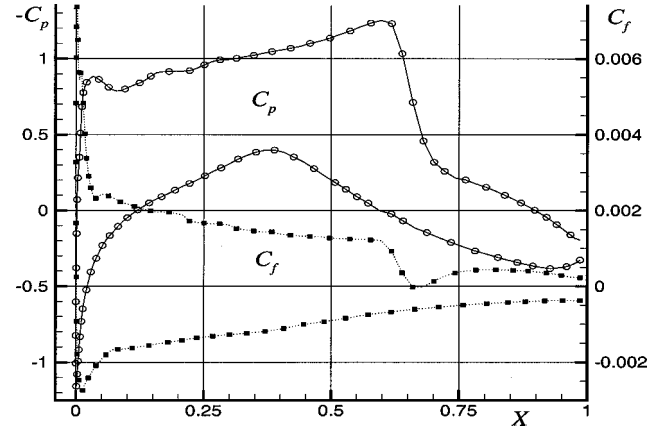

Fig. 9 Pressure and skin-friction coefficient distributions; turbulent airfoil inverse design.

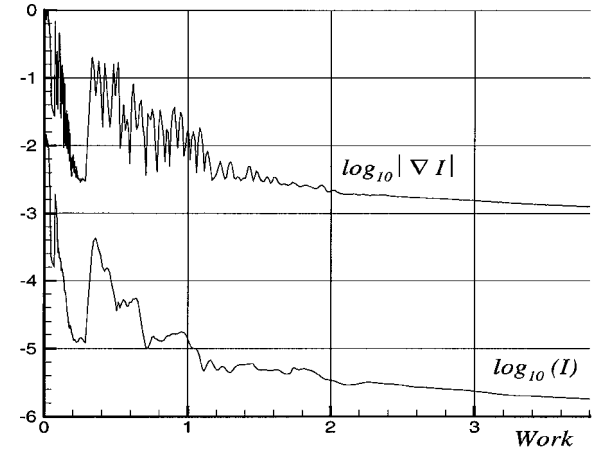

Fig. 10 Convergence history; turbulent airfoil inverse design, finest mesh: 256 × 64 cells.

units. In this test case, with coarser grids, the convergence achieved on the intermediate mesh is not as good as the one obtained by employing the finer grids. Therefore, the computational work required has increased, but it is still very low. Note the work reduction that can be obtained by using more refined meshes.

To test the influence of the number of design variables, we considered an optimization test with only one design variable, that is, $N_a = 1$ and Y_1, to be the ordinates of a NACA 0012 airfoil. The initial α_1 value was set to 2.5, which corresponds to considering an initial NACA 0030 airfoil configuration. The optimization process has been performed by employing three mesh levels made by 64×16, 128×32, and 256×64 cells. The corresponding convergence results indicate that the work required to converge the gradient of the objective function by 2.5 orders of magnitude is equal to 0.15. The work required is slightly lower than the work required to converge the four design variable test case, thus providing evidence that the number of design variables does not significantly alter the rapid convergence properties of the present methodology.

When the one design variable test case was recomputed by employing three coarser mesh levels made by 32×8, 64×16, and 128×32 cells, the corresponding convergence results indicate that the work required to converge the gradient of the objective function by 2.5 orders of magnitude was equal to 0.40. We observe again that the computational work required has increased with respect to the work required by the optimization process employing three finer mesh levels. We also observe that the work required is even slightly larger than the work required to converge the corresponding four-design variable test case, thus enforcing again the conclusion that the number of design variables does not significantly alter the efficient convergence properties of the present methodology.

In the present situation, we also performed an extended optimization test to investigate the ability of the inviscid adjoint formulation to bring the optimization process to machine zero. The convergence history is plotted in Fig. 8, which shows the capability of the present inviscid adjoint formulation to bring the optimization process to machine zero. The objective function decreases 12 orders of magnitude, and the modulus of the gradient of the objective function decreases more than 6 order of magnitude. In addition, the design variable approaches its target value with a relative error lower than 10^{-6}.

Turbulent Flow Airfoil Results

The inverse design of airfoils in turbulent flow conditions is now considered. The airfoil surface shape is described again by Eq. (17), where the weighting terms α_i continue to be the design parameters.

We considered the transonic turbulent flow about a Royal Aircraft Establishment (RAE) 2822 airfoil with an undisturbed Mach number $M_\infty = 0.75$ at an angle of attack equal to 2 deg and with a Reynolds number equal to 6.2×10^6 (cf., Ref. 20). Then the converged flowfield is evaluated by employing a C grid made by 256×64 cells with the first mesh point off of the surface corresponding to a $y^+ \leq 1$. The computed pressure and skin-friction coefficient distributions on the airfoil surface are plotted in Fig. 9 (continuous and dotted lines). This surface pressure distribution is taken to be the target pressure for our inverse design problem.

We performed an optimization test with $N_a = 4$ and Y_1–Y_4 as the shape of four specified airfoils, NACA 0012, RAE 2822, NACA 64_2A215, and NACA $65_2 - 415$. The target set of coefficients is $\alpha = (0, 1, 0, 0)$, and we assumed an initial airfoil shape corresponding to the set of coefficients $\alpha = (0.5, 1.5, 0.5, 0.5)$. The optimization process has been performed by employing three mesh levels made by 64×16, 128×32, and 256×64 cells.

Figure 10 shows the convergence history and indicates that the work required to converge the gradient of the objective function by 2.5 orders of magnitude is equal to 1.62. In this turbulent test case, the presence of a shock in the flowfield requires many more iterations on the finest mesh level, particularly in the very sensitive shock region, and consequently requires much more work with respect to the laminar flow test case. The corresponding optimal distributions of the pressure coefficient and of the skin-friction coefficient are plotted in Fig. 9 as symbols. Figure 9 shows good agreement between the target and the optimal distributions, indicating that the solution has converged sufficiently. Another indication of convergence can be observed in Fig. 11, where the target airfoil shape (continuous line) is plotted together with the initial airfoil shape (dashed line) and the optimized airfoil shape (symbols). Figure 11 shows that the optimized airfoil shape practically coincides with its target value. Figure 11 also illustrates that the optimization process starts from an airfoil shape very different from the optimized one.

To analyze the influence of the mesh size, the preceding optimization process has been repeated by employing the three coarser mesh levels made by 32×8, 64×16, and 128×32 cells. The initial and target α values were not changed. The corresponding convergence results indicate that the work required to converge the gradient of

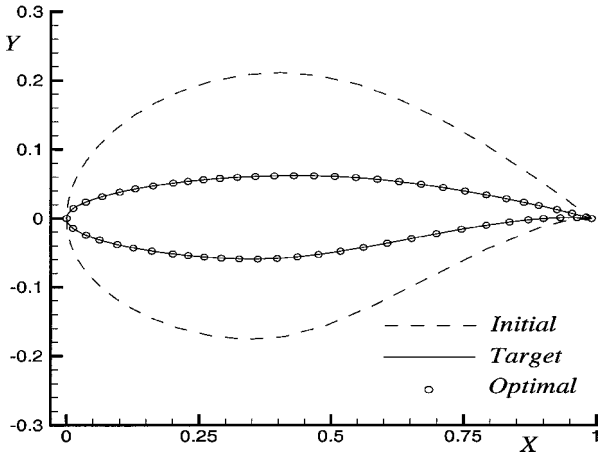

Fig. 11 Airfoil shapes; turbulent airfoil inverse design.

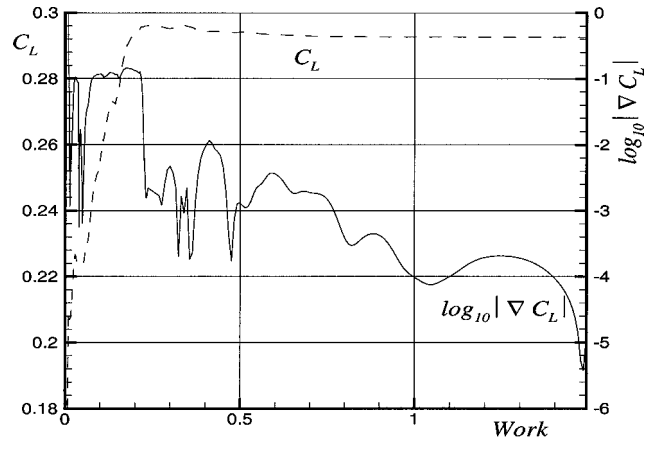

Fig. 12 Convergence history; laminar airfoil direct design, finest mesh: 256 × 64 cells.

the objective function by 2.5 orders of magnitude is equal to 2.14, higher than the work required using the more refined mesh levels. The conclusions drawn from the laminar inverse test case still appear to hold: The use of more refined mesh distributions leads to a work reduction.

Airfoil Direct Design

The direct design method that we implement is based on trying to determine the shape of an airfoil that optimizes a particular aerodynamic characteristic subject to several constraints. In the following, we will first describe the variations of the formulation with respect to the methodology outlined earlier. Then we will present results for airfoil designs corresponding to laminar as well as turbulent flow conditions.

Formulation

The only change in the formulation of the direct design problem involves the handling of constraints. All of the direct airfoil designs considered here will have an area constraint such that the airfoil cross-sectional area $A(\xi)$, nondimensionalized by c^2, with c the airfoil chord,

$$A(\xi) \geq A_{\min} \tag{18}$$

This area constraint has been directly enforced using a gradient projection method (cf., Ref. 21).

For the laminar direct design, we maximize the lift coefficient $C_L(\xi)$ with a constraint on the drag coefficient $C_D(\xi)$:

$$C_D(\xi) \leq C_{D\max} \tag{19}$$

We handle the constraint with a penalty function technique that minimizes the following objective function:

$$I(\xi) = -C_L + R_1\delta_1(C_D/C_{D\max} - 1)^2 \tag{20}$$

where δ_1 is equal to 0 for $C_D \leq C_{D\max}$ and is otherwise equal to 1. Also, R_1 is the penalty constant, which can be used to increase emphasis on the constraint violations.

For the turbulent direct design, we will maximize L/D. Effectively, this is performed by minimizing $C_D(\xi)/C_L(\xi)$, with the following constraint on the lift coefficient:

$$C_L(\xi) \geq C_{L\min} \tag{21}$$

The corresponding unconstrained optimization problem is to minimize the objective function

$$I(\xi) = C_D/C_L + R_2\delta_2(C_{L\min}/C_L - 1)^2 \tag{22}$$

where δ_2 is equal to 0 for $C_L \geq C_{L\min}$ and is otherwise equal to 1. R_2 is the penalty constant.

The δ_i terms are discontinuous at $C_D = C_{D\max}$ (laminar test case) or at $C_L = C_{L\min}$ (turbulent test case). Numerical experiments have shown this discontinuity to cause irregularities, which reduce the efficiency of the progressive methodology. As a consequence, we used an extended penalty function technique, which smooths such a discontinuity approximating the δ_i terms with a hyperbola.

The progressive optimization strategy outlined earlier is used with minor variations. Specifically, the optimization problem is considered to be completed when the norm of the gradient of the lift coefficient (laminar test case) or of the ratio $C_D(\xi)/C_L(\xi)$ (turbulent test case) is decreased 3.5 orders of magnitude with respect to the value it assumes in the early stages of the optimization process.

Laminar Flow Results

The test case analyzed in Ref. 22, extended to laminar flow, is considered here (i.e., we consider a laminar flowfield with an undisturbed Mach number equal to 0.75) at an angle of attack of 4 deg and with a Reynolds number equal to 5×10^2. The airfoil shape is described by Eq. (17) with $N_a = 4$. The terms Y_1–Y_4 are the shape of four specified airfoils, NACA 2412, NACA 64_1-412, NACA 64_2A215, and NACA 65_2-415. The initial airfoil shape corresponds to the set of coefficients $\alpha = (1, 0, 0, 0)$, that is, the constrained lift optimization process has been performed starting from a NACA 2412 airfoil. The minimum nondimensional area is taken to be $A_{\min} = 0.075$ and the drag coefficient constrained to be less than $C_{D\max} = 0.21$. The optimization process uses three mesh levels with 64×16, 128×32, and 256×64 cells.

Figure 12 presents the convergence history of the lift coefficient C_L and of the logarithm (base 10) of its normalized gradient, $\log_{10}|\nabla C_L|$, vs the work. The results indicate that the work required to converge the gradient of the lift coefficient by 3.5 orders of magnitude is equal to 0.93 work units. The computed lift coefficient is $C_L = 0.293$, whereas the drag constraint is very slightly violated at a value of $C_D = 0.213$. The area constraint is exactly enforced. Figure 12 shows that an apparent higher value of C_L is attained at the earlier stages of the convergence process, which is due to a flow solution that has not fully converged. The corresponding original NACA 2412 airfoil has a lift coefficient $C_L = 0.201$ and a drag coefficient $C_D = 0.220$. The optimization process has improved the lift coefficient by 46%, while reducing the drag coefficient by 3.3%. Unfortunately, the corresponding airfoil profile is rather unrealistic, as shown in Fig. 13, where the optimized profile is plotted. Figure 14 presents the pressure and skin-friction coefficient distributions. The unrealistic airfoil profile corresponds to a laminar flow point design. Obviously, at off-design conditions, this airfoil would perform poorly. More constraints would be required to produce a more realistic shape. However, the test case shows the ability of the methodology to improve the airfoil aerodynamic characteristics.

Turbulent Flow Results

Here we consider the lift over drag maximization starting from the RAE 2822 airfoil considered in the turbulent flow inverse design.

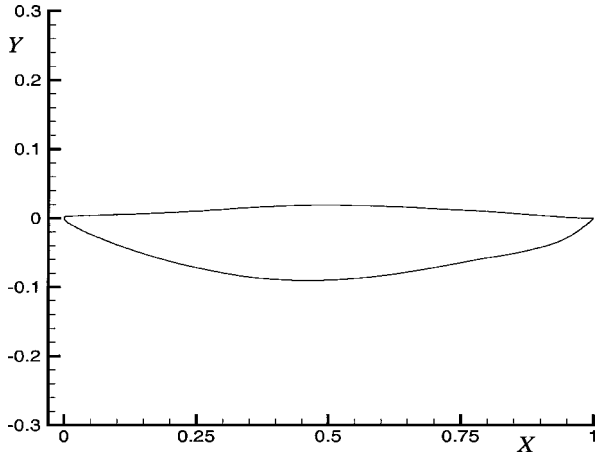

Fig. 13 Airfoil shape; laminar airfoil direct design.

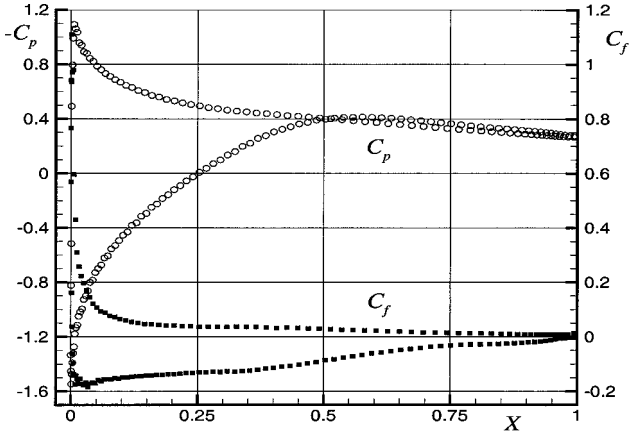

Fig. 14 Pressure and skin-friction coefficient distributions; laminar airfoil direct design.

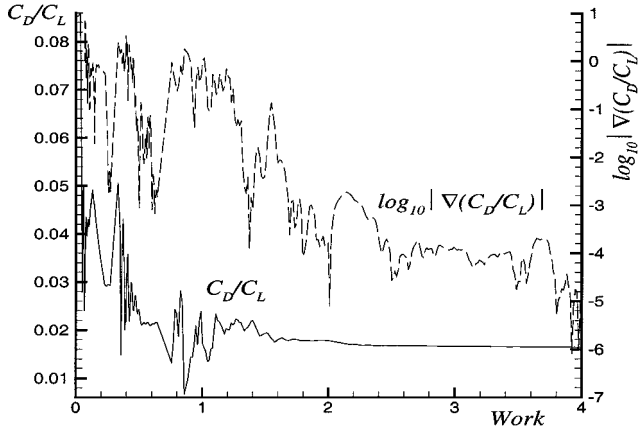

Fig. 15 Convergence history; turbulent airfoil direct design, finest mesh: 256 × 64 cells.

The undisturbed Mach number is equal to 0.75, the angle of attack is 2 deg, and the Reynolds number is equal to 6.2×10^6. The airfoil shape is described by Eq. (17) with $N_a = 4$. The terms Y_1–Y_4 are the shape of four specified airfoils, NACA 0012, RAE 2822, Korn airfoil, and NACA $65_2 - 415$. The initial airfoil shape corresponds to the set of coefficients $\alpha = (0, 1, 0, 0)$. The minimum nondimensional area is taken to be the area of the original RAE 2822 airfoil, and the minimum lift coefficient is taken to be $C_{L\,\min} = 0.65$. We performed a drag over lift minimization using three mesh levels: 64×16, 128×32, and 256×64 cells.

Figure 15 presents the convergence history of the drag over lift coefficients, C_D/C_L, and of the logarithm (base 10) of its normalized gradient, $\log_{10}|\nabla(C_D/C_L)|$, vs the work. The results indicate that the work required to converge the gradient of C_D/C_L by 3.5 orders of magnitude is equal to 2.38. The computed lift coefficient is $C_L = 0.7091$, and the drag coefficient is $C_D = 0.01164$, which correspond to a lift over drag $C_L/C_D = 60.9$. The area constraint is exactly enforced. For comparison, the corresponding original RAE 2822 airfoil shows a lift coefficient $C_L = 0.7212$ and a drag coefficient $C_D = 0.0185$, which correspond to a lift over drag $C_L/C_D = 39.0$. The optimization process has improved the lift over drag by 56%, with a very slight reduction in lift coefficient by 1.7%. The corresponding airfoil profile is shown in Fig. 16, which presents the optimized airfoil profile (continuous line) together with the original RAE 2822 airfoil profile (dashed line) and the airfoil profile at the beginning of the optimization process on the finest employed grid (dotted line). Figure 16 indicates the advantage of progressively refining the mesh for turbulent flow direct design. We see that the airfoil profile at the beginning of the optimization process on the finest employed grid is midway between the optimized and the original airfoil. The changes are particularly evident on the upper side of the airfoil, in the very sensitive shock region. Therefore, a substantial change in the airfoil profile has been obtained by utilizing coarser meshes at a low computational cost.

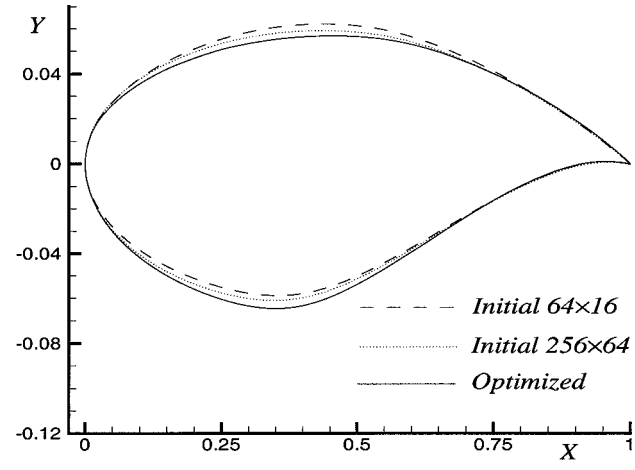

Fig. 16 Airfoil shape; turbulent airfoil direct design.

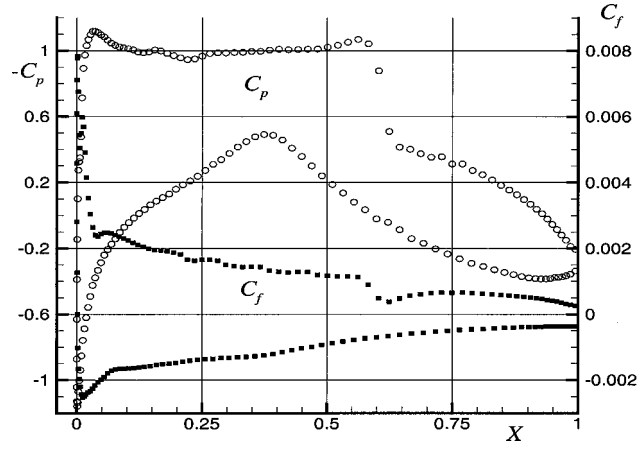

Fig. 17 Pressure and skin-friction coefficient distributions; turbulent airfoil direct design.

Finally, Fig. 17 presents the pressure and skin-friction coefficient distributions, which indicate that the optimized airfoil flow is characterized by a weak shock. The Mach number in front of the shock is approximately 1.35 on the original RAE 2822 airfoil, whereas it reduces to approximately 1.2 for the optimized airfoil.

To analyze the influence of the mesh size, the preceding optimization process has been repeated by employing the usual three coarser mesh levels made by 32×8, 64×16, and 128×32 cells. The convergence results indicate that the work required to converge the gradient of C_D/C_L by 3.5 orders of magnitude is equal to 2.52, 5% higher than the work required by the optimization performed

Table 1 Summary of viscous test cases

Test case	Design variation, N_a	Flow finest mesh	Work
Laminar inverse design	4	256×64	0.19
Laminar inverse design	4	128×32	0.37
Laminar inverse design	1	256×64	0.15
Laminar inverse design	1	128×32	0.40
Turbulent inverse design	4	256×64	1.62
Turbulent inverse design	4	128×32	2.14
Laminar direct design	4	256×64	0.93
Turbulent direct design	4	256×64	2.38
Turbulent direct design	4	128×32	2.52

with the finer mesh levels. In addition, the less accurate flow computations indicate an increase of the lift over drag, C_L/C_D, of only 31%. These results show that the use of finer mesh distributions improves the efficiency of the present methodology and the performance of the optimization.

Summary of Results

The results from the viscous test cases considered in this paper are summarized in Table 1.

These test cases give an indication of the applicability and efficiency of the design strategy described in this paper. Large gains in efficiency have been obtained through the progressive optimization strategy that utilized coarse grid solutions of an inviscid adjoint problem to obtain approximations for design sensitivities in viscous airfoil design problems. These cases included both inverse and direct designs of airfoils in laminar and turbulent flow. Over this class of applications, the methodology was highly efficient and exhibited robustness.

Conclusions

An extremely efficient formulation for the inverse and direct design optimization of airfoils in laminar and turbulent flow conditions is presented. Converged designs have been obtained in the computational work to perform less than two flow analyses on the finest grid, independent of the number of design variables. Our procedure simultaneously relies on converging the design process, the analysis, and the adjoint equation solution, while sequentially using progressively finer grids. Approximate design sensitivities are computed using a highly efficient adjoint solution procedure based on a simplified auxiliary flow solver. This simplified adjoint solution, based on an inviscid flow model that is artificially dissipative, is used only to generate approximate design sensitivities. The flow solution and the objective function are evaluated with standard Navier–Stokes solvers. Our procedure is implemented using what we term progressive optimization, whereby a sequence of operations, containing a partially converged flow solution, followed by a partially converged adjoint solution, followed by an optimization step, is performed. We utilize a sequence of finer grids for the flowfield solution, and use the coarsest grid for the solution of the adjoint equations.

This approach has been tested on inverse and direct (constrained) design problems involving airfoils in laminar and turbulent flow conditions. The methodology has exhibited robustness and was shown to be highly efficient, with a converged design optimization produced in no more than the amount of computational work to perform two flow analyses on the finest mesh. Parametric studies have shown that the relative work (based on a converged flow analysis on the finest grid) required to converge the optimization problems reduces using finer grids and is not significantly affected by the number of design variables.

The nature of our approach has been heuristic and has been substantiated on a sequence of test problems. The speed-up gains that we have observed using our methods are substantial. However, we have not attempted to assess the isolated gains of the individual elements of our procedures for the viscous design problems considered here. Furthermore, because our approach is based on the use of approximate sensitivity derivatives, we cannot ensure that the method will converge for every conceivable design problem However, for design problems such as those presented in this paper, we have not encountered any cases that have failed to converge or that even converge slowly.

Acknowledgments

The research of the first author has been supported by the Italian Agency Ministero dell'Istruzione, dell' Università e della Ricerca. The research of the second author was partially supported by the Air Force Office of Scientific Research through Grant F49620-96-1-0329.

References

[1]Dadone, A., and Grossman, B., "Progressive Optimization of Inverse Fluid Dynamic Design Problems," *Computers and Fluids*, Vol. 29, No. 1, 2000, pp. 1–32.

[2]Dadone, A., Valorani, M., and Grossman, B., "Optimization of Fluid Design Problems with Nonsmooth or Noisy Objective Function," *AIAA Journal*, Vol. 38, No. 3, 2000, pp. 418–426.

[3]Dadone, A., and Grossman, B., "Rapid Convergence of Airfoil Design Problems Using Progressive Optimization," *Lecture Notes in Physics*, Vol. 515, Springer, New York, 1998, pp. 25–30.

[4]Dadone, A., and Grossman, B., "CFD Design Problems Using Progressive Optimization," AIAA Paper 99-3295, June 1999.

[5]Dadone, A., and Grossman, B., "Fast Convergence of Inviscid Fluid Dynamic Design Problems," European Congress on Computational Methods in Applied Sciences and Engineering, Barcelona, Spain, Sept. 2000; also *Computers and Fluids* (to be published).

[6]Matsuzawa, T., and Hafez, M., "Approximate Gradients for Airfoil Design via Optimal Control," AIAA Paper 99-3105, June 1999.

[7]Alexandrov, N. M., Lewis, R. M., Gumbert, C. R., Green, L. L., and Newman, P. A., "Optimization Models with Variable-Fidelity Applied to Wing Design," AIAA Paper 2000-0841, Jan. 2000.

[8]Alexandrov, N. M., Nielsen, E. J., Lewis, R. M., and Anderson, W. K., "First-Order Model Management with Variable-Fidelity Physics Applied to Multielement Airfoil Optimization," AIAA Paper 2000-4886, Sept. 2000.

[9]Roe, P. L., "Characteristic Based Schemes for the Euler Equations," *Annual Review of Fluid Mechanics*, Vol. 18, 1986, pp. 337–365.

[10]Van Leer, B., "Towards the Ultimate Conservative Difference Scheme, V. A Second-Order Sequel to Godunov's Method," *Journal of Computational Physics*, Vol. 32, No. 1, 1979, pp. 101–136.

[11]Van Albada, G. B., Van Leer, B., and Robers, W. W., Jr., "A Comparative Study of Computational Methods in Cosmic Gasdynamics," *Astronomy and Astrophysics*, Vol. 108, No. 1, 1982, pp. 76–84.

[12]Baldwin, B. S., and Lomax, H., "Thin Layer Approximation and Algebraic Model for Separated Turbulent Flows," AIAA Paper 78-0257, 1978.

[13]Degani, D., and Shiff, L. B., "Computation of Supersonic Viscous Flows Around Pointed Bodies at Large Incidence," AIAA Paper 83-0034, 1983.

[14]Catalano, L. A., and Dadone, A., "Progressive Optimization for the Efficient Design of Three-Dimensional Cascades," AIAA Paper 2001-2578, June 2001.

[15]Catalano, L. A., and Dadone, A., "Progressive Optimization for the Inverse Design of Two-Dimensional Cascades," AIAA Paper 2000-3204, July 2000.

[16]Catalano, L. A., Dadone, A., Manodoro, D., and Saponaro, A., "Design Optimization and Validation of Improved Duct-Burners for Combined-Cycle Plants," American Society of Mechanical Engineers, ASME 2001 International Joint Power Generation Conf., Paper IJPGC PWR-19026, New Orleans, LA, June 2001.

[17]Iollo, A., Kuruvila, G., and Ta'asan, S., "Pseudo-Time Method for Optimal Shape Design Using the Euler Equations," ICASE, Rept. 95-59, Hampton, VA, 1995.

[18]Joh, C. Y., Grossman, B., and Haftka, R. T., "Design Optimization of Transonic Airfoils," *Engineering Optimization*, Vol. 21, No. 1, 1983, pp. 1640–1647.

[19]Bristeau, M. O., Glowinski, R., Periaux, J., and Viviand, A. (eds.), "Numerical Simulation of Compressible Navier–Stokes Flows," Vol. 18, Notes on Numerical Fluid Mechanics, Springer-Verlag, Berlin, 1987, pp. 3, 192, 193.

[20]Cook, P. H., McDonald, M. A., and Firmin, M. C. P., "Aerofoil RAE 2822—Pressure Distributions, and Boundary Layer and Wake Measurements," AR-138, AGARD, 1979, pp. A6.1–A6.77.

[21]Haftka, R. T., and Gürdal, Z., *Elements of Structural Optimization: Third Revised and Expanded Edition*, Kluwer Academic, Norwell, MA, 1992, pp. 176–182.

[22]Shenoy, A. T., "Optimization Technique Exploiting Problem Structure: Application to Aerodynamic Design," Ph.D. Dissertation, Aerospace and Ocean Engineering Dept., Virginia Polytechnic Inst. and State Univ., Blacksburg, VA, 1997, URL: http://scholar.lib.vt.edu/theses/available/etd-402101939761081/

E. Livne
Associate Editor